nature catalysis

Article

https://doi.org/10.1038/s41929-023-01068-2

Stereoselective construction of β-, γ- and δ-lactam rings via enzymatic C–H amidation

Received: 11 January 2023

Accepted: 23 October 2023

Published online: 6 December 2023

Check for updates

Satyajit Roy[1,5,7], David A. Vargas[1,6,7], Pengchen Ma[2,3,7], Arkajyoti Sengupta[2], Ledong Zhu[4], K. N. Houk[2] ✉ & Rudi Fasan[1,5] ✉

Lactam rings are found in many biologically active natural products and pharmaceuticals, including important classes of antibiotics. Methods for the asymmetric synthesis of these molecules are therefore highly desirable, particularly through the selective functionalization of unreactive aliphatic C–H bonds. Here we show the development of a strategy for the asymmetric synthesis of β-, γ- and δ-lactams via the haemoprotein-catalysed intramolecular C–H amidation of readily accessible dioxazolone reagents. Engineered myoglobin variants serve as excellent biocatalysts for this transformation, yielding the desired lactam products in high yields with high enantioselectivity and on a preparative scale. Mechanistic and computational studies were conducted to elucidate the nature of the C–H amidation and enantiodetermining steps and provide insights into the protein-mediated control of the regioselectivity and stereoselectivity. Additionally, an alkaloid natural product and a drug molecule were synthesized chemoenzymatically in fewer steps (7–8 versus 11–12) than previously reported, further demonstrating the power of biosynthetic strategies for the preparation of complex bioactive molecules.

The selective functionalization of ubiquitous yet unreactive carbon–hydrogen (C–H) bonds via both chemical and enzymatic methods constitutes a powerful strategy for the diversification of organic molecules and enabling the devising of new disconnections and routes for the construction of complex molecules and natural products[1–7]. Owing to the high prevalence of amine-based functionalities in bioactive molecules and pharmaceuticals, a highly desirable and sought-after transformation in organic and medicinal chemistry is the selective amination of aliphatic C–H bonds[8–10]. Notable advances in this field have led to the development of organometallic catalysts for catalysing the insertion of nitrene species into C–H bonds, resulting in the formation of new carbon–nitrogen bonds (Fig. 1b)[8–10]. These transformations are mediated by reactive metal–nitrenoid species generated by reaction of the transition metal catalyst with nitrene precursor reagents such as iminoiodinanes, azides and hydroxylamine derivatives[8–10]. Using this strategy, a variety of cyclic amines, including oxazolidinones, sulfamates, sultams and pyrrolidines, have been accessed. Despite this progress, the extension of this C–H amination strategy to the synthesis of cyclic amides (lactams), which are key structural motifs in many pharmaceuticals, agrochemicals and other fine chemicals (Fig. 1a)[11,12], has represented a major challenge[13]. The difficulty of this transformation can be attributed to the instability of the acyl nitrene intermediate, which can undergo facile decomposition to isocyanates through a Curtius-type rearrangement, thereby outcompeting the desired C–H nitrene insertion process[13]. Recently, Chang and co-workers reported a breakthrough in this area through the development of an iridium-based catalyst system that enables this transformation[13]. This progress notwithstanding, asymmetric versions of this methodology

[1]Department of Chemistry, University of Rochester, Rochester, NY, USA. [2]Department of Chemistry and Biochemistry, University of California, Los Angeles, CA, USA. [3]School of Chemistry, Xi'an Key Laboratory of Sustainable Energy Materials Chemistry, MOE Key Laboratory for Nonequilibrium Synthesis and Modulation of Condensed Matter, Xi'an Jiaotong University, Xi'an, China. [4]Environment Research Institute, Shandong University, Qingdao, People's Republic of China. [5]Present address: Department of Chemistry and Biochemistry, University of Texas at Dallas, Richardson, TX, USA. [6]Present address: Process Research and Development, Merck, Rahway, NJ, USA. [7]These authors contributed equally: Satyajit Roy, David A. Vargas, Pengchen Ma. ✉e-mail: houk@chem.ucla.edu; rudi.fasan@utdallas.edu

https://doi.org/10.1038/s41929-023-01068-2

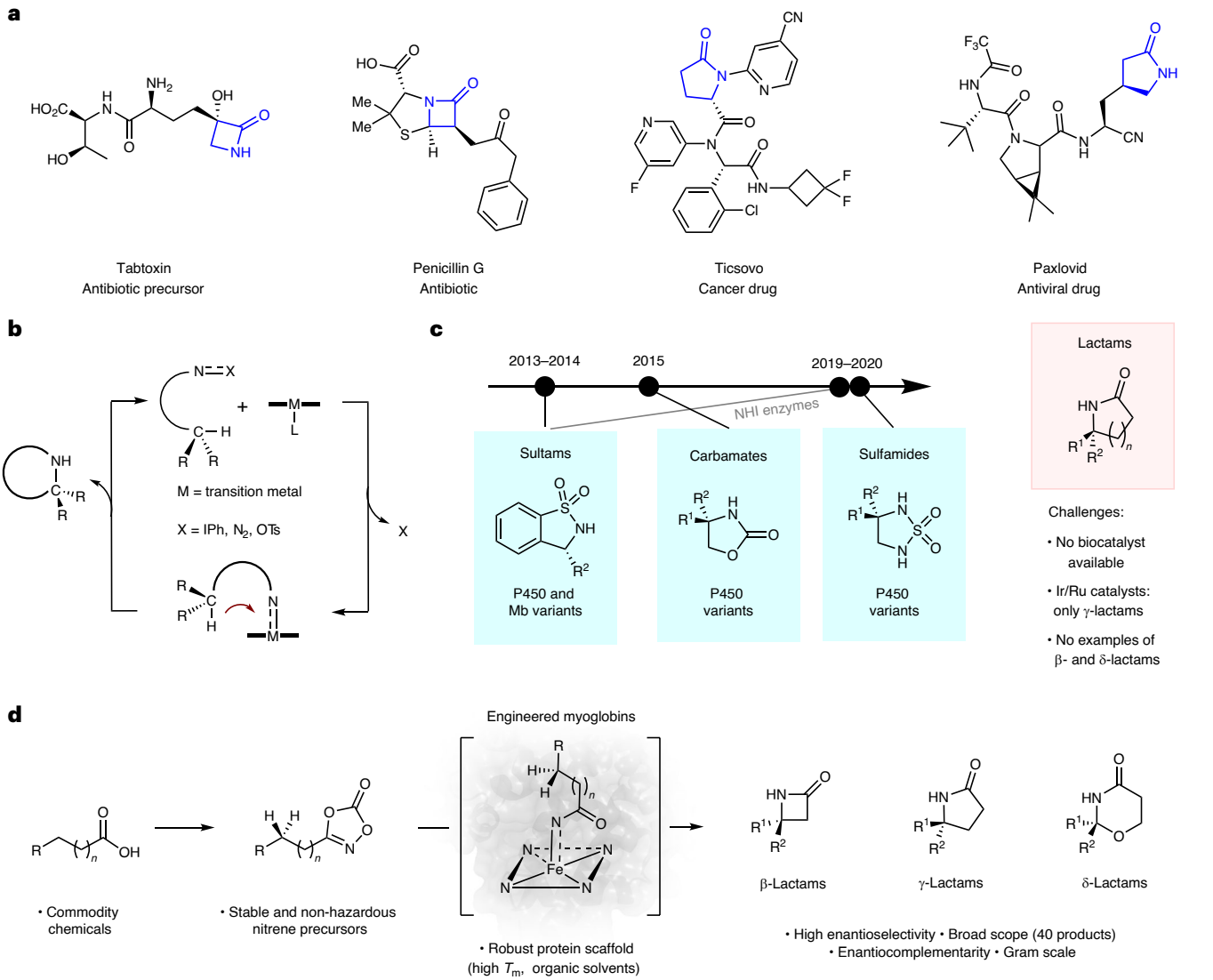

Fig. 1 | Asymmetric lactam synthesis via enzyme-catalysed C(sp^3)–H amidation. a, Bioactive molecules containing β- and γ-lactam rings. **b**, General catalytic cycle for C–N bond formation via nitrene transfer. **c**, Enzyme-catalysed intramolecular C–H amination reactions. NHI denotes non-haem iron-dependent enzymes. **d**, Biocatalytic construction of β-, γ- and δ-lactam rings via myoglobin-catalysed intramolecular C–H amidation of dioxazolones (this work).

are restricted to five-membered rings (γ-lactams) and require the use of rare and toxic metals (that is, Ir and Ru)[14,15].

Inspired by the chemistry of metalloporphyrins[16], our group and the Arnold group have recently demonstrated the ability of engineered haemoproteins to serve as biocatalysts for intramolecular[17–22] and intermolecular[23–25] C–H amination reactions via nitrene transfer (Fig. 1c). Specifically, engineered cytochrome P450 (hereafter denoted P450) enzymes have been shown to catalyse the cyclization of sulfonyl azides, carbonazidates and sulfonazidates[22] to produce sultams, cyclic carbamates and cyclic sulfamides, respectively[17–22]. Furthermore, iridium-substituted P450s[26] and non-haem Fe-dependent enzymes[27,28] were also found to catalyse similar intramolecular C–H amination reactions. Despite this progress, the synthesis of lactam rings using biocatalytic nitrene transfer approaches has remained elusive, largely due to the aforementioned difficulty in controlling the reactivity of acyl nitrene intermediates while disfavouring other competing, unproductive reactions (for example, nitrene reduction) known to affect these abiological enzyme-catalysed reactions[21].

Here we report the development of a general biocatalytic methodology for the asymmetric synthesis of enantioenriched lactams via the intramolecular C–H amidation of dioxazolones (Fig. 1d), a safe and readily accessible class of nitrene donor reagents[29]. This strategy provides an efficient and scalable approach to the selective construction of γ-lactam molecules with high enantioselectivity. Furthermore, the scope of this biocatalytic system can be extended to the construction of optically active β- and δ-lactam motifs with high enantiocontrol. The power of this methodology is further showcased through the concise chemoenzymatic total synthesis of an alkaloid natural product and a drug molecule. Comprehensive mechanistic studies were conducted to elucidate the nature of the C–H amidation step, as well as the role of the protein scaffold in controlling the regio- and enantioselectivity of the reaction. Leveraging a direct C–H amidation strategy, this methodology is mechanistically distinct, yet complementary to recently reported biocatalytic approaches for γ-lactam synthesis that rely on the radical-mediated cyclization of alkene-containing substrates[30–32] or carbene C–H insertion with artificial enzymes[33].

Results

Biocatalyst discovery

Inspired by the previous work of Chang and co-workers[13,34], we envisioned the possibility of executing an enzyme-catalysed γ-C–H amidation reaction via nitrene transfer using dioxazolone reagent **1a**

https://doi.org/10.1038/s41929-023-01068-2

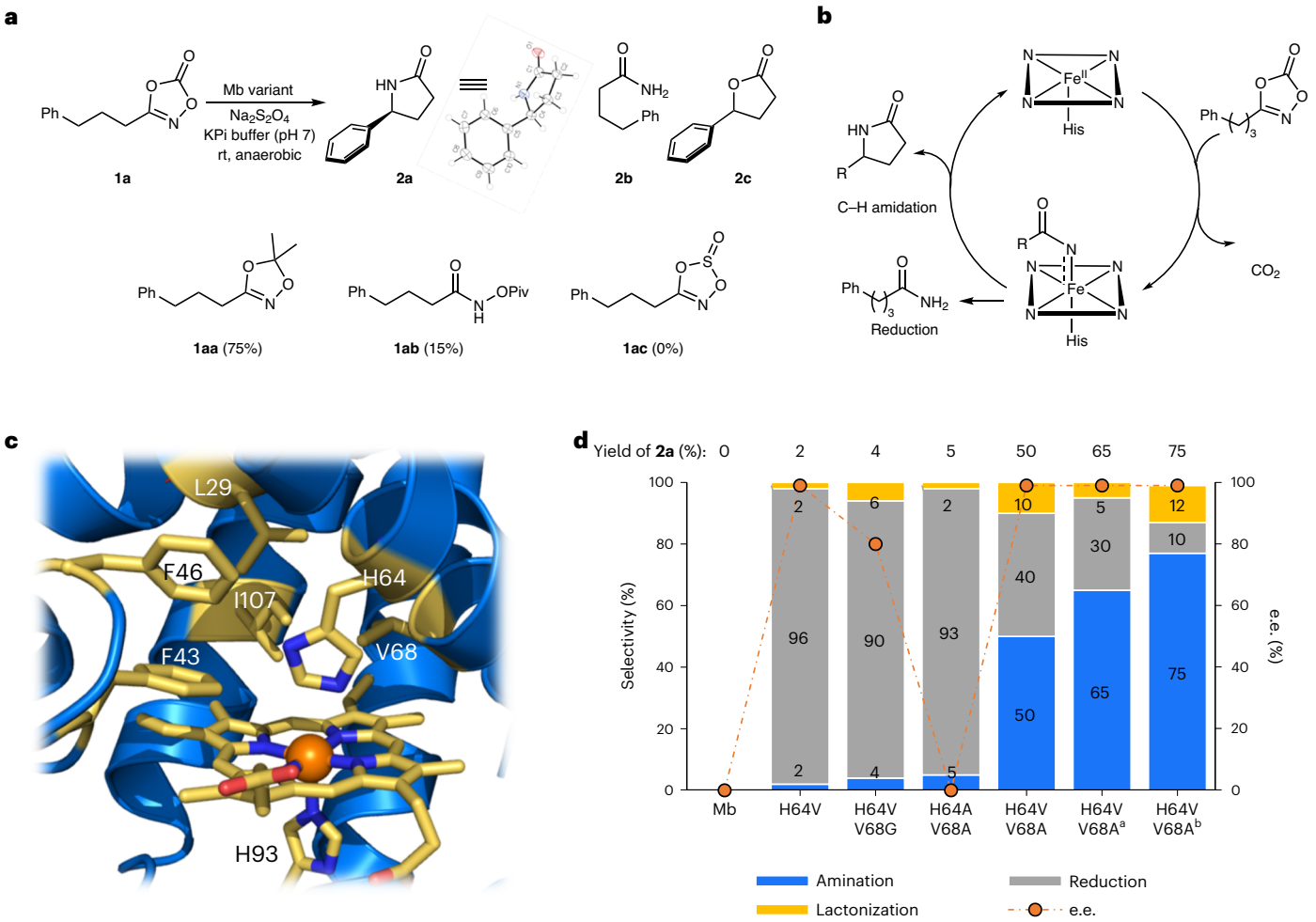

Fig. 2 | Biocatalytic intramolecular C(sp^3)–H amidation of dioxazolones. **a**, Amidation reaction of 3-phenylpropyldioxazolone **1a**. The X-ray crystal structure of the desired product **2a** is shown. Structures are shown of alternative nitrene precursors **1aa**, **1ab** and **1ac** along with the corresponding yields of the product **2a** (in parentheses) using Mb* under the standard reaction conditions. KPi, potassium phosphate; rt, room temperature. **b**, Envisioned haemoprotein-catalysed nitrene transfer process for γ-lactam ring formation. **c**, Crystal structure of wild-type Mb (Protein Data Bank entry 1JW8) with the residues near the Fe centre highlighted in yellow. **d**, Activity, chemoselectivity and enantioselectivity (for **2a**) of engineered Mb variants in the reaction with **1a**. Reaction conditions: 20 μM protein, 10 mM **1a**, 10 mM $Na_2S_2O_4$ in potassium phosphate buffer (50 mM, pH 7), 3 h, room temperature, anaerobic conditions. The yields and product distribution were determined by GC using calibration curves of the isolated product. [a]With acetonitrile as co-solvent. [b]Using sodium borate buffer (pH 9) with 5% (v/v) acetonitrile (equivalent to the standard reaction conditions).

(Fig. 2a,b). Particularly attractive features of dioxazolones as nitrene precursors include their facile synthesis from commodity carboxylic acids and their stability and safety compared with the azide-based reagents previously used in biocatalytic nitrene transfer reactions[17–22]. To identify an initial biocatalyst for this reaction, we tested various haem-containing enzymes and proteins, including wild-type myoglobin (Mb), P450s, peroxidases and cytochromes *c*, under anaerobic conditions (Supplementary Table 1). Many of these reactions produced the acyclic amide **2b** as a by-product, with none of these biocatalysts displaying any activity towards the formation of the desired γ-lactam product (Supplementary Table 1). Previous studies by our group demonstrated that mutations of the distal His64 residue in Mb (Fig. 2c) can enhance its activity towards non-native carbene and nitrene transfer reactions[35,36]. Promisingly, Mb(H64V) was found to react with **1a** to yield minute yet detectable amounts of the desired lactam **2a** (2% yield by gas chromatography (GC)) with good levels of enantioselectivity (96% e.e.; Fig. 2d).

Encouraged by these results, we extended the screening to a broader panel of engineered Mb variants (Supplementary Table 2) containing mutations at the distal His64 residue (Ala, Val or Gly) along with additional mutations within the active site of the haemoprotein (Fig. 2c). From this screening, multiple Mb variants were found to exhibit increased C–H amidation activity compared with Mb(H64V) (10–50% yields; Supplementary Table 2). Among them, Mb(H64V,V68A) (denoted Mb*), which was previously developed for stereoselective cyclopropanation[35], emerged as the best biocatalyst for this reaction, producing **2a** in 50% yield with excellent enantioselectivity (>99% e.e.; Fig. 2d). The configuration of the γ-lactam product was determined to be *S* by crystallography (Fig. 2a and Supplementary Fig. 11). In addition to the C–H amidation product, the Mb*-catalysed reaction also produced a notable amount (40%) of the amide by-product **2b** (Fig. 2a), which probably arises from the reduction and protonation of the nitrene intermediate (Supplementary Fig. 15), as observed previously for C–H amination reactions with azide-based precursors[18,22]. Unexpectedly, a minor product (10%), corresponding to the γ-lactone **2c**, was also formed in the reaction (Fig. 2a).

Method optimization

Compared with Mb*, Mb variants containing Ala and/or Gly mutations at the 64 or 68 positions showed significant decreases in activity and/or

selectivity (Supplementary Table 2, entries 3–6 versus 7), and a similar effect was observed on the introduction of additional mutations into Mb*, suggesting that the reaction is sensitive to subtle changes in the shape of the enzyme's active site. Based on previous mechanistic studies on P450-mediated C–H amination[21] and given the robustness of Mb biocatalysts towards organic solvents[37], we hypothesized that the addition of an organic co-solvent could favour the desired C–H amidation reaction by disfavouring the formation of the amide by-product **2b**. Accordingly, the screening of various organic co-solvents showed that acetonitrile was beneficial for increasing the yield of the C–H amidation product (from 50% to 65%), while reducing the undesired reduction reaction (30%) and without affecting the enantioselectivity (Fig. 2d and Supplementary Fig. 1). Further optimization of the reaction conditions revealed that slightly alkaline conditions (pH 9) further increased the C–H amidation activity (75% yield of **2a**) of the enzyme at the expense of by-product **2b** (10%), while retaining excellent enantioselectivity (Fig. 2d). These trends are consistent with our hypothesis that the formation of the amide by-product **2b** involves protonation of the nitrene intermediate, which should be disfavoured under more alkaline conditions and in the presence of organic solvent. Under limiting catalytic conditions (0.07 mol%), Mb* was determined to catalyse the C–H amidation of **1a** to produce **2a** in 58% yield with a turnover number of 2,175 and excellent enantioselectivity. In addition to dioxazolone **1a**, we also evaluated other nitrene precursors, such as dioxazole **1aa**, acyl-protected hydroxylamine **1ab** and dioxathiazole **1ac** (Fig. 2a). Although **1ac** and **1ab** were inactive or less effective than **1a**, respectively, in the cyclization reaction (Fig. 2c), dioxazole **1aa** produced the desired γ-lactam product in good yield (75% **2a**), thereby constituting another viable nitrene precursor for this biocatalytic C–H amidation strategy.

Substrate scope

To assess the substrate scope of this methodology, Mb* was tested against an array of substituted dioxazolone substrates (**1d**–**p**). As summarized in Fig. 3a, these experiments revealed a high tolerance of the enzyme towards substitutions at the *para* position of the aryl ring, affording the desired γ-lactam products (**2d**–**i**) with high-to-excellent enantioselectivity (73–99% e.e.). While both electron-withdrawing and -donating substitutions were accepted by the enzyme, increased activity was observed for substrates containing electron-donating substituents (**1h**,**i**). Substitutions at the *ortho* and *meta* positions were also well tolerated by the enzyme, producing the corresponding γ-lactam products (**2j**–**l**) in good yields (68–88%) and high enantiopurity (99% e.e.; Fig. 3a). In addition to substituted phenyl groups, the enzyme catalysed the cyclization of substrates containing heteroaryl groups, such as thiophenyl (**1m**,**n**), with good-to-high levels of activity (75–90% yields) and enantioselectivity (66–99% e.e.). Furthermore, the enzymatic synthesis of **2p** in 28% yield with an 83:17 diastereomeric ratio also showed the tolerance of the enzyme towards substitutions at the α-position of the dioxazolone core. Allylic C–H amidation was also possible, as demonstrated by the successful preparation of **2o** in 38% yield and 99% e.e. from **1o** (7:3 *E*/*Z* mixture), with other products of these reactions corresponding only to the reduction (amide) byproducts. Notably, the double bond in **1o** showed no reactivity in this reaction, which highlights the chemoselectivity of the iron-based biocatalyst towards C–H nitrene insertion over aziridination, typically favoured by Rh-based catalysts in nitrene transfer reactions[38]. Last, isoindolinones **10** and **12** were successfully obtained from the cyclization of phenyldioxazolones **9** and **11**, respectively (Supplementary Fig. 14), albeit in high yield but no enantioselectivity (**10**) or with high enantioselectivity but low yield (**12**). Conversely, dioxazolone substrates lacking an aromatic group (for example, **16** and **17**; Supplementary Fig. 14) or containing bulky aryl substituents proximal to the γ-C–H bond (for example, **15** and **18**; Supplementary Fig. 14) eluded Mb*-catalysed C–H amidation, indicating that further optimization of the biocatalyst for these types of substrate would be required in the future.

Enantiodivergent biocatalyst

Enantiodivergent biocatalysts are highly desirable, yet often hard to develop[39]. Notably, screening of the initial Mb active-site mutant library revealed a variant, Mb(L29T,H64V,V68L), that catalyses the cyclization of **1a** with inverted enantioselectivity compared with Mb*, producing the *R*-configured γ-lactam product ***ent*-2a** in 65% e.e., albeit in modest yield (15%; Supplementary Table 2). To improve the performance of this biocatalyst, Mb(L29T,H64V,V68L) was subjected to active-site mutagenesis, ultimately leading to Mb(L29T,H64T,V68L), which produced ***ent*-2a** with both an improved enantioselectivity of 91% e.e. and twofold higher activity compared with the parent enzyme. To explore the substrate promiscuity of this enantiocomplementary biocatalyst, Mb(L29T,H64T,V68L) was tested against dioxazolones **1d**–**p**. Albeit in more moderate yields compared with the reactions performed with Mb*, the majority of these substrates (9 of 13) were converted into the *R*-configured γ-lactam products with good-to-high enantioselectivity (57–99% e.e.; Fig. 3a). Of note, ***ent*-2k**, ***ent*-2l** and the thiophenyl-containing substrate ***ent*-2m** were all obtained with 99% e.e. These results highlight the broad substrate scope and predictable enantiocomplementarity of the two Mb-based biocatalysts for γ-lactam ring formation.

Synthesis of β- and δ-lactams

Next, we targeted the synthesis of β-lactams, which are highly desirable building blocks for medicinal chemistry as well as key pharmacophores in β-lactam antibiotics[12]. Notably, β-lactam formation via intramolecular nitrene transfer has not been reported to date. On treating substrate **3a** with Mb*, the desired β-lactam **4a** was obtained in high yield (85%) and excellent enantioselectivity (99% e.e.; Fig. 3b). Mirroring the *S* enantioselectivity in γ-lactam formation, the enzyme was observed to maintain *S* enantiopreference in the formation of **4j**, as determined by X-ray crystallography (Fig. 3b). These findings prompted us to explore the substrate scope of this reaction with dioxoazolones **3b**–**j** (Fig. 3b). Remarkably, the variously substituted substrates were converted into the desired β-lactam products with excellent enantioselectivity (99% e.e.; Fig. 3b) and yields of up to 93%. Unlike the γ-lactams, substrates bearing electron-withdrawing groups on the aryl ring cyclized more efficiently than those containing electron-donating groups (for example, 32% yield for **4d** versus 75% for **4c**), and *meta* substitutions were better tolerated than *para* substitutions (for example, 75% yield for **4g** versus 32% for **4d**). These differences probably arise from the differential role of electronic and steric constraints in the four- and five-membered ring formation. The furanyl- and thiophenyl-containing substrates **3i** and **3j**, respectively, also cyclized very efficiently (75% and 93% yields, respectively) with high enantiocontrol (99% e.e.).

Next, we explored the activity of the Mb biocatalyst for the synthesis of δ-lactams. The reaction of substrate **5a** resulted in a mixture of δ-lactam **6aa** and γ-lactam **6ab** in a 1:3.7 ratio, in addition to the amide **6b** as the major product (7:26:67 ratio for **6aa**/**6ab**/**6b**; Fig. 3c). These results reveal the preference of the enzyme for the amidation of the homobenzylic γ-C–H bond (to give **6ab**) over the benzylic δ-C–H bond (to give **6aa**), despite the higher bond dissociation energy of the former (~95 versus 90 kcal mol^{-1}; Fig. 3c). While the formation of both the γ- and δ-lactam products (3.7:1 ratio) suggests that the enzyme's regioselectivity could be tuned via protein engineering, these findings inspired us to steer the enzyme's regioselectivity via substrate engineering, that is, by substituting the γ-C–H with an O atom to favour δ-lactam formation (Fig. 3c). Gratifyingly, the reaction of Mb* with the corresponding substrate **5c** produced the desired δ-lactam **6c** with significantly improved efficiency (78% yield) as well as excellent enantioselectivity (99% e.e.; Fig. 3c). This biocatalytic reaction was found to be compatible also with substitutions on the aryl ring, as demonstrated by the synthesis of the δ-lactams **6d**–**f** in 45–93% yields and high enantioselectivity (93–99% e.e.). In addition, benzoxazinone **14** was obtained in high yield from the

https://doi.org/10.1038/s41929-023-01068-2

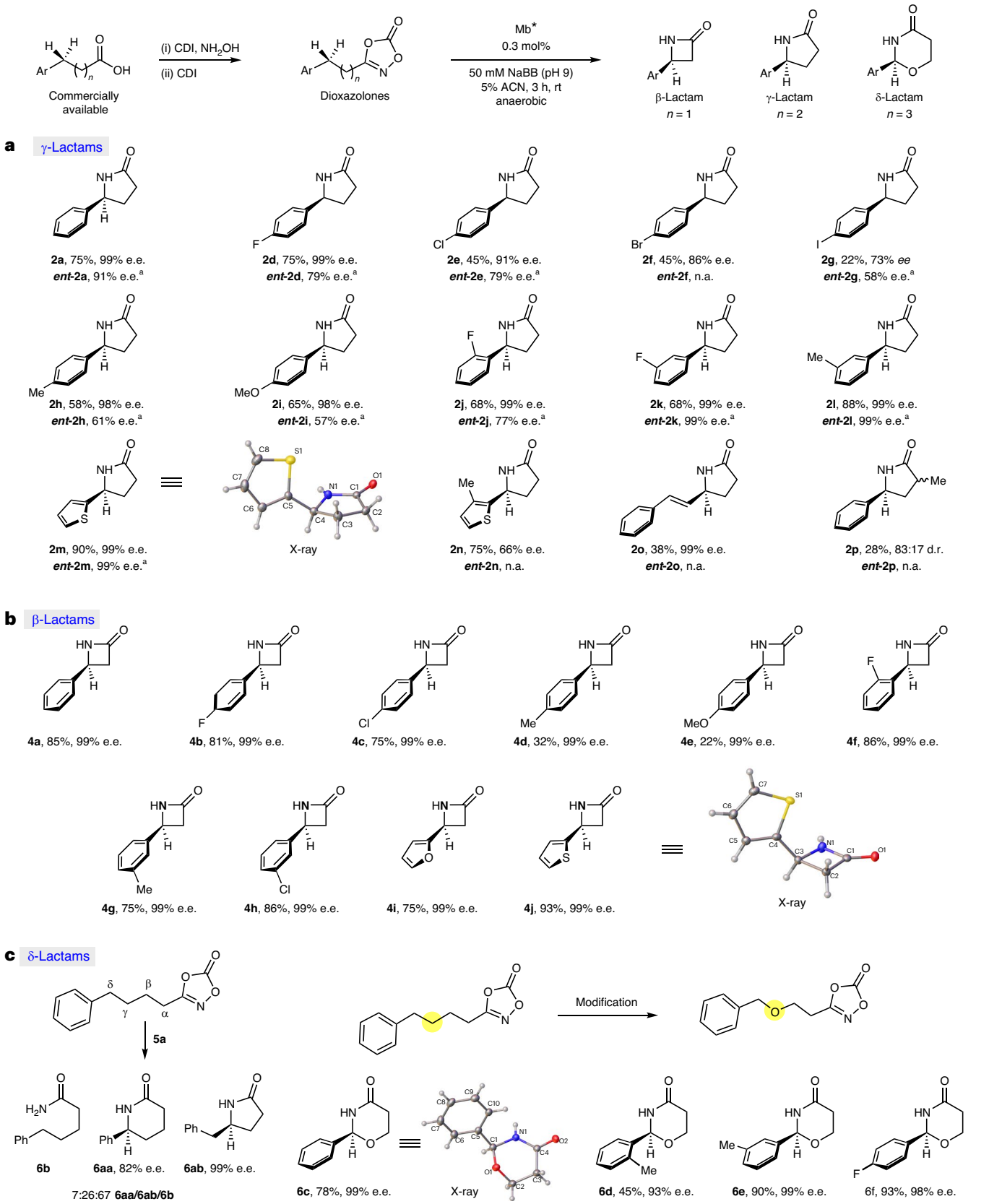

Fig. 3 | Substrate scope for Mb*-catalysed C–H amidation reaction. a–**c**, Substrate scope of the Mb*-catalysed C–H amidation of dioxazolones for the synthesis of lactams with various ring sizes: γ-lactams (**a**), β-lactams (**b**) and δ-lactams (**c**). [a]Using Mb(L29T,H64T,V68L) as the catalyst. CDI, carbonyldiimidazole; NaBB, sodium borate buffer; n.a., not active.

Mb*-catalysed cyclization of 3-phenyldioxazolone-based substrate **13**, albeit only in racemic form (Supplementary Fig. 14).

Taken together, these results reveal a remarkable generality of the Mb* catalyst towards enabling the stereoselective synthesis of lactams of varying sizes and with different substitutions. Also noteworthy is the consistent and predictable *S* stereoselectivity of the Mb*-catalysed C–H amidation reaction, not only across the different substrates but also across β-, γ- and δ-lactam rings, which adds to the synthetic utility of this biocatalytic system.

Mechanistic studies

Studies were then performed to gain insights into the mechanism of this enzyme-catalysed reaction. To probe the nature of the C–H amidation step, the Mb*-catalysed reaction was carried out with the *Z*-configured dioxazolone **1q**, which resulted in the formation of the *E*-configured lactam **2q** (Fig. 4a). This result rules out a concerted C–H nitrene insertion process and is consistent with a stepwise hydrogen atom abstraction (HAA)–radical rebound mechanism proceeding via an allylic radical that undergoes $Z \rightarrow E$ isomerization to yield ***trans*-2q** before radical recombination. Of note, the complete isomerization of the double bond in the cyclization product (no ***cis*-2q** was observed) shows that the radical intermediate is relatively long-lived.

To further investigate the kinetic role of the C–H cleavage step, non-competitive intermolecular H/D competition experiments were carried out using substrate **1a** and **1a-d_2** in parallel reactions (Fig. 4b). These experiments yielded a kinetic isotope effect (KIE) value of 2.6 ± 0.2 (Fig. 4b and Supplementary Fig. 3), which is lower than those determined for C–H amination reactions with azide-based substrates catalysed by engineered P450s (k_H/k_D = 3.4–5.3)[20,40], but higher than those determined for the P450-catalysed cyclization of sulfonyl azides (k_H/k_D = 0.9), where the azide activation was established to be rate-determining[21]. Overall, these results indicate that the C–H cleavage step in the present system is only partially rate-determining, with other steps contributing to control the overall rate of the reaction.

To gain insight into the enantiodetermining step(s) in this reaction, isotopomeric dioxazolones **(*S*)-1a-d_1** and **(*R*)-1a-d_1** were synthesized in enantiopure form (Supplementary Fig. 4) and subjected to Mb*-catalysed C–H amidation. Interestingly, both reactions led to the accumulation of deuterated lactam **(*S*)-2a-d_1** as the predominant product over the protiated counterpart **(*S*)-2a** (ratios of 95:5 and 98:2 from **(*S*)-1a-d_1** and **(*R*)-1a-d_1**, respectively), as determined by NMR spectroscopy (Fig. 4c and Supplementary Fig. 4). In addition, both reactions proceeded with high enantioselectivity (99% e.e.). Two conclusions can be derived from these results: first, H abstraction is strongly favoured over D abstraction, regardless of the configuration of the C–H amination site, and second, protein-mediated enantioinduction in the C–N bond-forming process must occur in the radical rebound step (Fig. 4d). Indeed, the formation of **(*S*)-2a-d_1** as the major product from both **(*S*)-1a-d_1** and **(*R*)-1a-d_1**, along with the preserved high e.e. in both cases, implies that, after HAA, the *pro-S* and *pro-R* conformations of the radical intermediate can undergo rapid interconversion, with the enzyme's active site enforcing radical rebound through the *pro-S* intermediate (*Si* face attack; Fig. 4c).

The $k_{H/D}$ values derived from the reactions of the isotopomeric substrates (Fig. 4c) result from a combination of the KIE (k_H/k_D) and the enzyme's enantiopreference in the HAA step (that is, k_S/k_R). The higher $k_{H/D}$ measured for the reaction of **(*R*)-1a-d_1** compared with for **(*S*)-1a-d_1** (49 versus 19) indicates a higher chirality match for H abstraction in **(*R*)-1a-d_1** compared with in **(*S*)-1a-d_1**, that is, the abstraction of $H^{pro\text{-}S}$ in **(*R*)-1a-d_1** is favoured by both the KIE and the enzyme, whereas the abstraction of $H^{pro\text{-}R}$ in **(*S*)-1a-d_1** is favoured by the KIE but disfavoured by the enzyme (Fig. 4d). Consistent with this chirality match effect, the amount of the reduction by-product (that is, **(*R*)-2a-d_1** or **(*S*)-2a-d_1**) compared with that of **2a** from the reaction with **1a** is slightly reduced (−5%) in the case of **(*R*)-1a-d_1** and markedly increased (+70%) in the case of **(*S*)-1a-d_1** (Fig. 4d). However, the mere 2.6-fold difference between the $k_{H/D}$ values for **(*R*)-1a-d_1** and **(*S*)-1a-d_1** (compared with the 50- to 220-fold difference determined for other systems[40,41]) suggests that the HAA step is barely stereoselective and thus that asymmetric induction is largely controlled by the enzyme during the radical recombination step. As such, this system shows a distinct enantioinduction mechanism from that described for asymmetric C–H aminations of sulfonyl azide substrates catalysed by Co porphyrins[41] and P411 catalysts[22,40].

Computational analysis of the reaction mechanism

Density functional theory (DFT) calculations were performed to explore the formation of the γ-lactam product **2a** from dioxazolone **1a**. The quintet (high spin), triplet (intermediate spin), closed-shell singlet (low spin) and open-shell singlet (low spin) spin states of each intermediate and transition-state structure were considered in the calculations. The energies of the lowest-energy spin state for different intermediates and transition-states are presented in Fig. 4e, with the energies of the other spin states given in Supplementary Fig. 5. The DFT calculations describe the iron–nitrenoid active species in this system as a triplet ground state, in analogy with other iron–nitrenoid species[22,25]. The calculations indicate that the formation of iron–nitrenoid complex **IM1** by activation of the dioxazolone substrate, with concomitant loss of CO_2, has an energy barrier of only 4.2 kcal mol^{-1} and involves an open-shell singlet spin state. After spin crossing, the HAA step is favoured in the triplet state, giving the carbon radical intermediate **IM2**, with an energy barrier of 8.0 kcal mol^{-1}. The following step, involving a radical rebound to give the final γ-lactam product, was found to be most favourable in the open-shell singlet state, with an energy barrier of 12.5 kcal mol^{-1}. The intermediate **IM2** has a high spin contamination (S^2 = 1.10), indicating that the open-shell singlet is not a pure singlet spin state, but 50:50 singlet/triplet, as is often observed in calculations on diradicals. Based on the energy profile, the C–N bond-forming step is predicted to be rate-determining, exhibiting a 4.5 kcal mol^{-1} higher energy barrier than the C–H bond-cleavage event. These findings are in excellent agreement with the results from the mechanistic experiments (Fig. 4) and explain the long-lived nature of the radical intermediate, as suggested by the complete double bond isomerization observed in ***trans*-2q** (Fig. 4a).

This mechanistic model also provides a framework for defining a plausible mechanism for the formation of the unexpected γ-lactone product **2c** from **1a** (Fig. 2a). After the HAA step, single electron transfer from the C-centred radical to the haem (or protein matrix) can generate a benzylic carbocation that can then react with the amide group (via the carbonyl group) to form a dihydrofuranimine ring. Hydrolysis of the latter produces **2c** (Supplementary Fig. 15). In addition to this radical–polar crossover mechanism, a radical pathway can be envisioned that proceeds via the same dihydrofuranimine intermediate, produced via reaction of the benzylic radical with the amidyl group (Supplementary Fig. 15). In either case, a slow C–N bond-forming radical rebound step, as revealed by our mechanistic and DFT studies, is expected to enable this competing side reaction to occur under sub-optimal reaction conditions.

Enzyme-controlled regio- and enantioselectivity

To investigate the role of the enzyme in controlling the enantioselectivity of the reaction, we explored the haem-bound iron–nitrenoid intermediate **IM1** docked in the active site of Mb* using the available crystal structure of this protein[42]. As shown in Fig. 5a, the N atom of **IM1** can abstract either H^1 or H^2, leading to the *S* or *R* lactam product, respectively, under fast radical rebound conditions. We measured the evolution of the distances between the N atom and the H^1 and H^2 atoms during 1,000 ns of molecular dynamics (MD) simulations (Fig. 5b). These studies showed that the average distances from the N atom to H^1 and H^2 are 3.96–4.01 and 4.06–4.10 Å, respectively, suggesting little to no preference for the abstraction of H^1 over H^2 (leading to the *S* or *R* product) by the nitrene intermediate.

https://doi.org/10.1038/s41929-023-01068-2

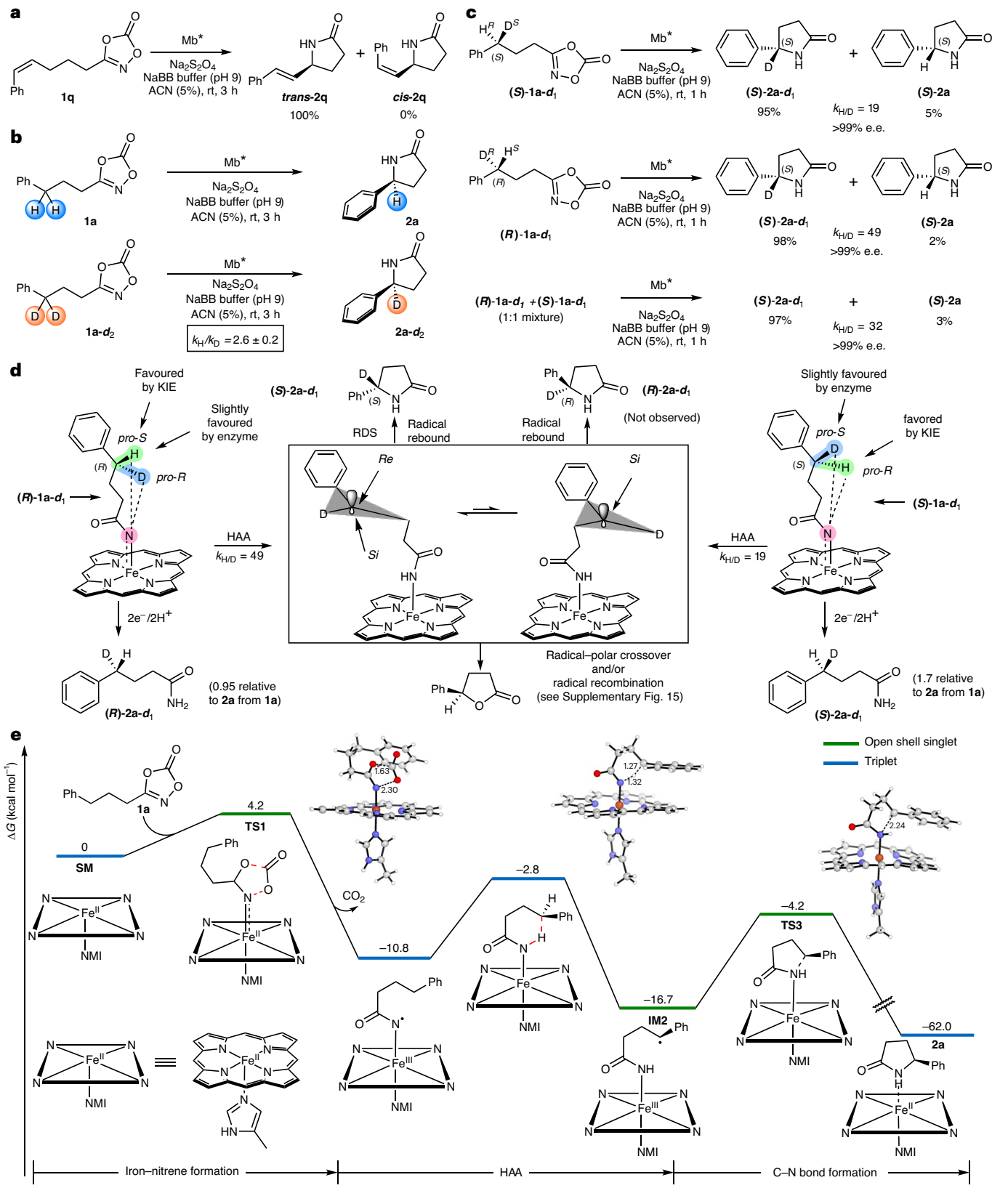

Fig. 4 | Mechanistic studies. a, Mb*-catalysed cyclization of substrate (*Z*)-**1q** shows complete isomerization to the *E* isomer product ***trans*-2p** (see Supplementary Fig. 2 for details). **b**, Non-competitive intermolecular KIE experiments, comparing the product formation rates of parallel reactions with protiated and deuterated substrates. See Supplementary Fig. 3 for details. **c**, H/D competition experiments with enantiopure isotopomeric dioxazolidones. $k_{H/D}$ values were determined by NMR spectroscopy (see Supplementary Fig. 4 for details). **d**, Mechanistic model for Mb*-controlled asymmetric induction. **e**, Gibbs free-energy diagram for Mb-catalysed γ-lactam formation. The Δ*G* values were calculated at the uB3LYP-D3BJ/def2tzvp(SMD,solvent = water)// uB3LYP-D3BJ/6-31G(d)+SDD(Fe) level of theory using a truncated computational model of the enzyme (Supplementary Fig. 5). See Supplementary Fig. 5 for additional spin states. Distances are in Å. NMI , 5-methylimidazole; SM, starting material; TS, transition state; IM, intermediate.

https://doi.org/10.1038/s41929-023-01068-2

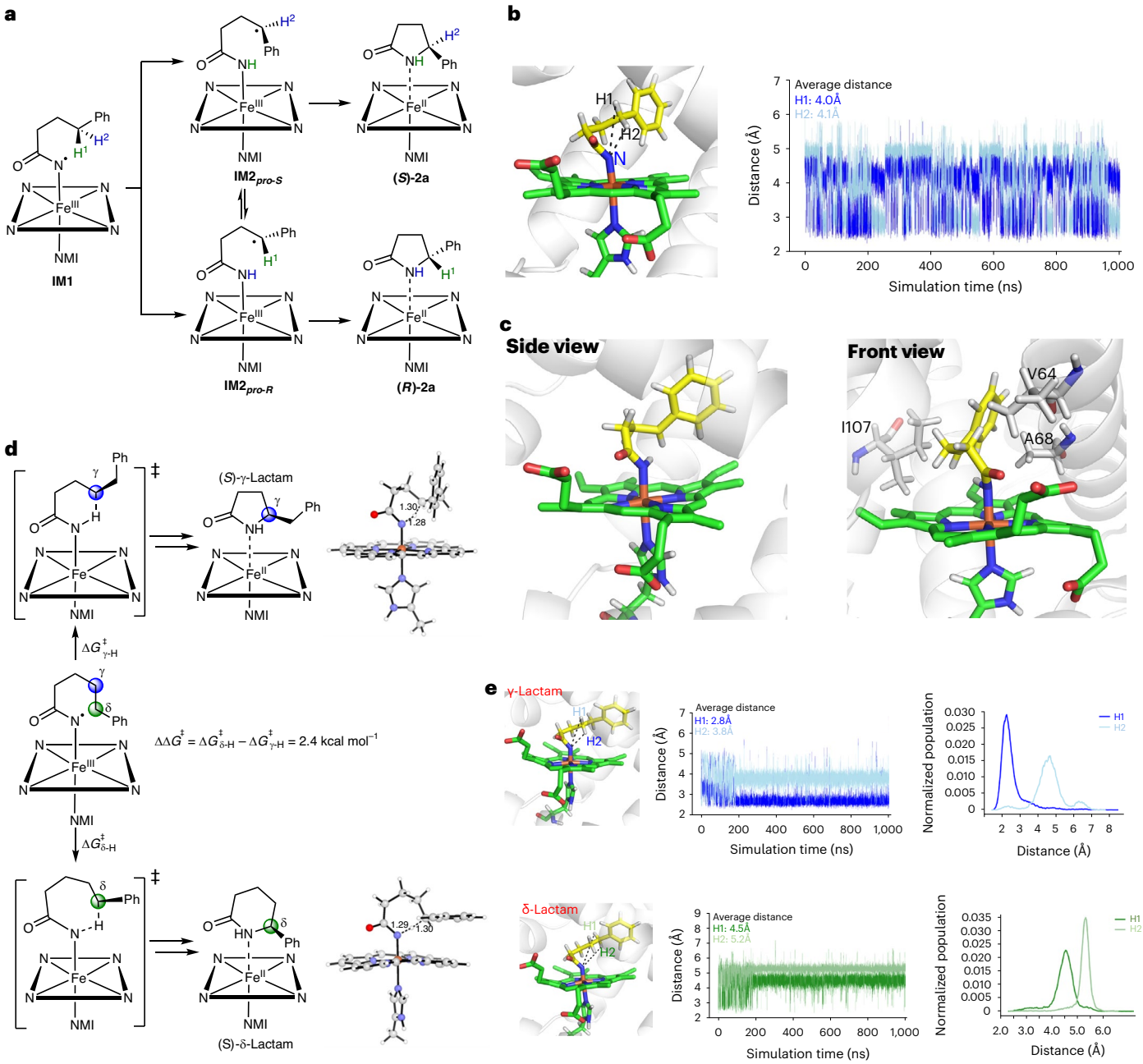

Fig. 5 | Computational analysis of the enantio- and regiocontrol. a, HAA step in the C–H amidation of **1a** to give the corresponding γ-lactam product **2a**. **b**, Representative snapshot of the intermediate **IM1** in the active site of Mb* (left) and plot of the nitrene N···H^1 and N···H^2 distances (right) over the 1,000 ns MD simulation. See Supplementary Fig. 6 for additional MD simulations. **c**, Side and front views of the most populated conformation of the benzylic radical intermediate **IM2** in the Mb* haem pocket over the entire 1,000 ns simulation. The key residues implicated in stabilizing the **IM2** conformation leading to the *S*-configured product **2a** after radical rebound are highlighted. **d**, Difference in the DFT-calculated energy barrier for γ- and δ-H atom abstraction in the nitrene intermediate **IM1** derived from substrate **5a**. The structures of the transition states are shown with key distances given in Å. **e**, Representative snapshots of **5a**-derived intermediate **IM1** in the active site of Mb* (left) and distance plots (middle) and Boltzmann distribution (right) of the nitrene N···γ-H and N···δ-H distances over the 1,000 ns MD simulation. See Supplementary Fig. 9 for additional MD simulations.

Next, the carbon radical intermediate **IM2** was docked in the active site of Mb* in a conformation that could lead to the *S* lactam product (**IM2$_{pro\text{-}S}$**) and a conformation that could lead to the *R* lactam product (**IM2$_{pro\text{-}R}$**), as shown in Supplementary Fig. 7. After MD simulations for 1,000 ns, both complexes converged to a conformation that favours radical rebound via the *Si* face of the benzylic radical species (Fig. 5c), leading to the (*S*)-γ-lactam **2a**. Inspection of this structure indicates that the active site residues Ile107, Val64 and Ala68 contribute to orient the haem-bound intermediate in the *pro-S* conformation. Furthermore, DFT calculations show that the transition state **TS3** for the formation of the *R*-configured product is disfavoured by 3.1 kcal mol^{-1} compared with that leading to the *S* product (Supplementary Fig. 8). This value of $\Delta\Delta G^{\ddagger}$ is consistent with the high *S* enantioselectivity induced by the enzyme (>99:1 e.r.) in the intramolecular C–H amidation reaction. The models for both the HAA and radical rebound step show the aryl ring projecting into the core of the protein between Ile107 and Ala68 (Fig. 5b,c). While this arrangement can accommodate substitution at different positions

https://doi.org/10.1038/s41929-023-01068-2

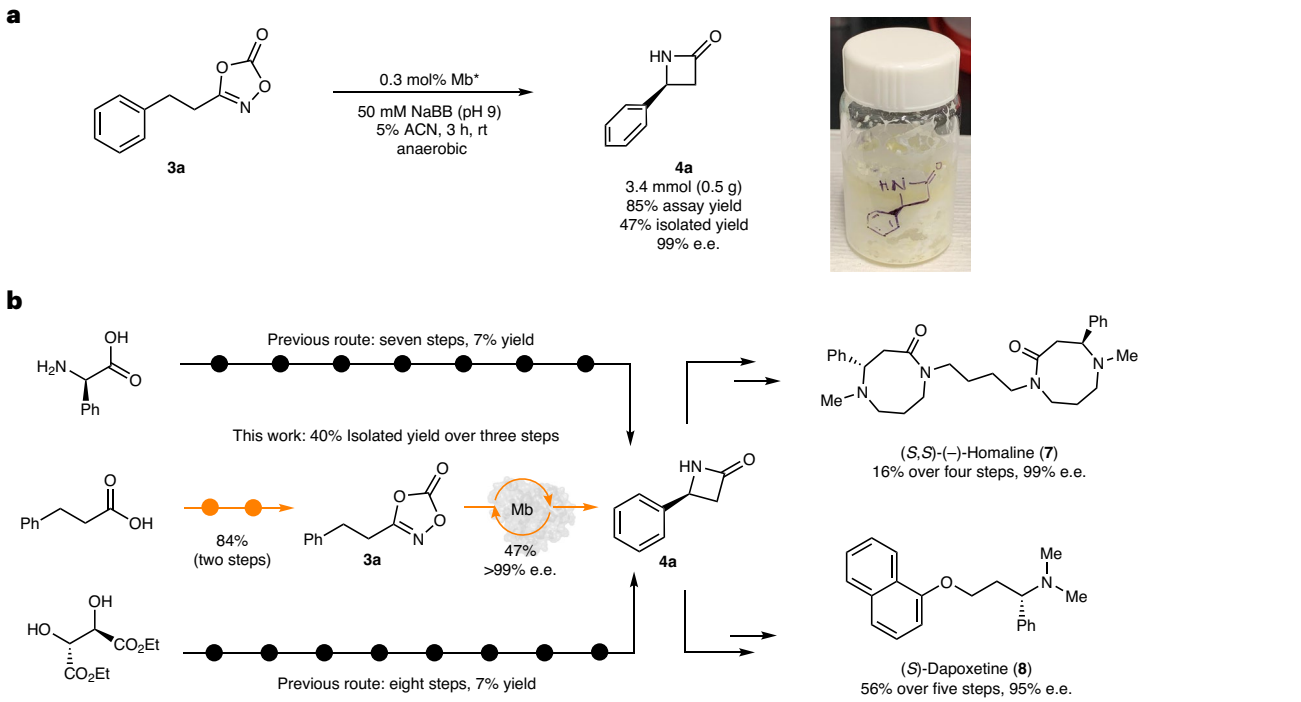

Fig. 6 | Applications of the Mb*-catalysed C–H amidation reaction. a, Gram-scale synthesis of β-lactam **4a**. **b**, Chemoenzymatic total synthesis of the alkaloid natural product (*S,S*)-(−)-homaline (**7**) and synthetic drug (*S*)-dapoxetine (**8**).

of the aryl ring, it also shows potential steric constraints as the size of the *para* substituent increases, providing a plausible rationale for the structure–activity trends observed experimentally (that is, -F (**2d**) > -Cl/Br (**2e**,**f**) > -I (**2g**); Fig. 4a).

To understand the regioselectivity of the enzyme, we studied the nitrene intermediate **IM1** generated from substrate **5a** (Fig. 5d). In this case, the nitrene intermediate can abstract either a γ- or δ-H atom, leading to the five- or six-membered lactam product, respectively. DFT calculations show that the energy barrier for hydrogen abstraction leading to the δ-lactam is 2.4 kcal mol^{-1} higher than that for the formation of the γ-lactam (Fig. 5d). We also studied the proximity of the γ- and δ-H atoms to the nitrene N atom through MD simulations over 1,000 ns. The γ-H···N average distance is 2.8–3.9 Å, whereas for δ-H···N, the distance is significantly longer at 4.3–5.2 Å (Fig. 5e and Supplementary Fig. 10). Thus, both the lower energy barrier for γ-H abstraction and the shorter nitrene N···γ-H atom distance contribute to favour the formation of the γ-lactam product, which can explain the regioselectivity of the Mb*-catalysed C–H amidation of **5a** observed experimentally (Fig. 3c).

Chemoenzymatic total synthesis of bioactive molecules

The present strategy was then applied to the chemoenzymatic synthesis of bioactive alkaloid (*S,S*)-(−)-homaline (**7**) and the Food and Drug Administration-approved drug (*S*)-dapoxetine (**8**; Fig. 6). Specifically, we envisioned that the key β-lactam intermediate **4a**, previously accessible only in low yields and after lengthy routes (seven to eight steps, 7% overall yield[43,44]; Fig. 6b), could be produced in a more efficient and step-economical manner by enzymatic means using the present method. Accordingly, enantiopure β-lactam **4a** (>99% e.e.) was produced from **3a** and isolated on a preparative scale (0.5 g) from a scaled up reaction with Mb* (Fig. 6a). From **4a**, (*S,S*)-(−)-homaline (**7**) and (*S*)-dapoxetine (**8**) could be synthesized in only four and five steps, respectively, using known routes (Fig. 6b; see Supplementary Fig. 16 for further details). Overall, asymmetric Mb-catalysed C–H amidation enabled the chemoenzymatic synthesis of the alkaloid natural product and drug molecule in a total of 7 and 8 steps, respectively, compared with the 11 and 12 steps required in previous total synthesis strategies. In addition, with the present approach, the key enantiopure β-lactam intermediate **4a** was readily obtained from the achiral, commodity chemical hydrocinnamic acid as opposed to the more expensive optically active precursors required in the previously reported routes (Fig. 6b). These results further showcase the synthetic utility and scalability of the present methodology for the synthesis of biologically active molecules.

Discussion

In summary, we have developed a biocatalytic strategy for the asymmetric construction of lactam molecules via nitrene transfer. Starting from readily accessible dioxazolones, this strategy could be leveraged to afford a broad range of β–, γ- and δ-lactam scaffolds in good yields and high enantioselectivity using a single Mb-based biocatalyst. In addition, we have demonstrated the possibility of obtaining enantiopodes of the γ-lactam products using an alternative engineered Mb variant with enantiodivergent selectivity. Our mechanistic investigations revealed that these reactions proceed via a HAA–radical rebound pathway, with the enzyme binding site controlling the stereo- and regioselectivity (β-, γ- and δ-C–H amidation) of the process. Furthermore, while the HAA step is generally assumed to be enantiodetermining in enzymatic C–H aminations[45,46], our studies show that the protein-induced enantioselectivity in the present system is largely controlled in the radical rebound step. The power of the present methodology is further showcased by the concise chemoenzymatic total synthesis of an alkaloid natural product and a drug molecule in around half as many steps as required previously, while offering higher overall yields and starting from a commodity chemical instead of optically active precursors. This work expands the available biocatalytic toolbox for the asymmetric synthesis of amine-containing molecules and paves the way to the development of other asymmetric enzyme-catalysed nitrene transfer reactions involving dioxazolones as nitrene precursors.

Methods

Molecular cloning

pET22b(+) (Novagen) was used as the recipient plasmid vector for expression of all of the myoglobin variants. In this construct, the Mb gene is carboxy-terminally fused to a polyhistidine tag and is under the control of an β-D-1-thiogalactopyranoside (IPTG)-inducible T7 promoter. The cloning of the Mb variants tested in this study has been described previously[47–49].

Protein expression and purification

The engineered Mb variants were expressed in *Escherichia coli* C41(DE3) or BL21(DE3) cells as described previously[47]. Briefly, cells were grown in terrific broth medium (100 mg l^{-1} ampicillin) at 37 °C (150 r.p.m.) until the optical density at 600 nm reached 0.9–1.2. The cells were then induced with 0.25 mM IPTG and 0.3 mM δ-aminolevulinic acid. After induction, the cultures were shaken at 180 r.p.m. and 27 °C and collected after 18–20 h by centrifugation at 4,000 r.p.m. at 4 °C. After cell lysis by sonication, the proteins were purified by Ni-affinity chromatography. The lysate was transferred to a nickel nitriloacetic acid (Ni-NTA) column equilibrated with Ni-NTA lysis buffer. The resin was washed with 50 ml Ni-NTA lysis buffer and then 50 ml Ni-NTA wash buffer (50 mM KPi buffer, 250 mM NaCl, 20 mM imidazole, pH 8.0). The proteins were eluted with Ni-NTA elution buffer (50 mM KPi buffer, 250 mM NaCl, 250 mM histidine, pH 7.0). After elution, the proteins were buffer-exchanged against 50 mM KPi buffer (pH 7.0 or 8.0) using 10 KDa Centricon filters. The myoglobin concentration was determined using the extinction coefficient for its Fe(III) form at 410 nm: $\varepsilon_{410} = 157\ mM^{-1}\ cm^{-1}$.

Purified protein reactions

Analytical reactions were carried out at the 400 µl scale using 20 µM myoglobin, 10 mM dioxazolone and 10 mM sodium dithionite under anaerobic conditions unless otherwise noted. In a typical procedure, 24-well plates or crimp vials containing a concentrated amount of Mb were introduced into an anaerobic chamber. Then, a corresponding amount of degassed KPi buffer (50 mM, pH 7.0) or NaBB (50 mM, pH 9) was added to each well or vial, followed by the addition of 40 µl sodium dithionite solution (100 mM stock solution) in KPi or NaBB to produce a 20 µM myoglobin solution. The reactions were initiated by the addition of 10 µl dioxazolone (400 mM stock solution in organic solvent). The plates were covered with aluminium foil (the vials were capped) and left shaking at 120 r.p.m. (or under magnetic agitation for vials) for 3–16 h at room temperature. The reactions were then analysed outside of the chamber following the protocol detailed below in Product analysis. Reactions with haemin or iron-tetraphenyl-porphyrin chloride (Fe(TPP)(Cl)) were carried out following an identical procedure with the exception that the purified Mb was replaced by haemin (20 µM in *N*,*N*-dimethylformamide) or Fe(TPP)(Cl) (20 µM in CH_2Cl_2).

Product analysis

Enzymatic reactions were analysed by adding 20 µl of internal standard (50 mM benzodioxole in ethanol) to the reaction mixture, followed by extraction in 400 µl CH_2Cl_2. The organic phase was analysed by GC with flame ionization detection (GC-FID) using a Shimadzu GC-2010 gas chromatograph equipped with an FID detector and a chiral Cyclosil-B column (30 m × 0.25 mm × 0.25 µm film) according to the following protocol: 1 µl injection, injector temperature: 250 °C, detector temperature: 300 °C, temperature gradient: column temperature set at 180 °C for 3 min, then raised to 185 °C at 1.0 °C min^{-1}, then to 190 °C at 2.0 °C min^{-1} then to 245 °C at 80 °C min^{-1} with a 0 min hold. The total run time was 16.19 min. The stereoselectivity was determined via chiral GC-FID and HPLC (see the Supporting Information for details). Assay yields were determined using calibration curves constructed with authentic standards prepared via preparative-scale reactions with purified Mb(H64V,V68A), as described in Synthetic procedures in the Supplementary Information. All measurements were performed at least in duplicate.

Reporting summary

Further information on research design is available in the Nature Portfolio Reporting Summary linked to this article.

Data availability

The crystallographic data of the small molecules have been deposited at the Cambridge Crystallographic Data Centre (CCDC) under deposition numbers CCDC 1893087 (**2a**), 2157011 (**2m**), 2157007 (**4j**) and 2157010 (**6c**). The data can be obtained free of charge via https://www.ccdc.cam.ac.uk/structures/.

References

1. Guillemard, L., Kaplaneris, N., Ackermann, L. & Johansson, M. J. Late-stage C–H functionalization offers new opportunities in drug discovery. *Nat. Rev. Chem.* **5**, 522–545 (2021).
2. Hong, B. K., Luo, T. P. & Lei, X. G. Late-stage diversification of natural products. *ACS Cent. Sci.* **6**, 622–635 (2020).
3. Gutekunst, W. R. & Baran, P. S. C–H functionalization logic in total synthesis. *Chem. Soc. Rev.* **40**, 1976–1991 (2011).
4. Wencel-Delord, J. & Glorius, F. C–H bond activation enables the rapid construction and late-stage diversification of functional molecules. *Nat. Chem.* **5**, 369–375 (2013).
5. Upp, D. M. & Lewis, J. C. Selective C–H bond functionalization using repurposed or artificial metalloenzymes. *Curr. Opin. Chem. Biol.* **37**, 48–55 (2017).
6. Ren, X. K. & Fasan, R. Engineered and artificial metalloenzymes for selective C–H functionalization. *Curr. Opin. Green Sustain. Chem.* **31**, 100494 (2021).
7. Chakrabarty, S., Wang, Y., Perkins, J. C. & Narayan, A. R. H. Scalable biocatalytic C–H oxyfunctionalization reactions. *Chem. Soc. Rev.* **49**, 8137–8155 (2020).
8. Roizen, J. L., Harvey, M. E. & Du Bois, J. Metal-catalyzed nitrogen-atom transfer methods for the oxidation of aliphatic C–H bonds. *Acc. Chem. Res.* **45**, 911–922 (2012).
9. Dequirez, G., Pons, V. & Dauban, P. Nitrene chemistry in organic synthesis: still in its infancy? *Angew. Chem. Int. Ed.* **51**, 7384–7395 (2012).
10. Park, Y., Kim, Y. & Chang, S. Transition metal-catalyzed C–H amination: scope, mechanism, and applications. *Chem. Rev.* **117**, 9247–9301 (2017).
11. Royer, J. *Chiral Amine Synthesis. Methods, Developments and Applications* (Wiley-VCH, 2010).
12. Tahlan, K. & Jensen, S. E. Origins of the β-lactam rings in natural products. *J. Antibiot.* **66**, 401–410 (2013).
13. Hong, S. Y. et al. Selective formation of γ-lactams via C–H amidation enabled by tailored iridium catalysts. *Science* **359**, 1016–1021 (2018).
14. Park, Y. & Chang, S. Asymmetric formation of γ-lactams via C–H amidation enabled by chiral hydrogen-bond-donor catalysts. *Nat. Catal.* **2**, 219–227 (2019).
15. Zhou, Z. J. et al. Non-C_2-symmetric chiral-at-ruthenium catalyst for highly efficient enantioselective intramolecular C(sp^3)–H amidation. *J. Am. Chem. Soc.* **141**, 19048–19057 (2019).
16. Breslow, R. & Gellman, S. H. Tosylamidation of cyclohexane by a cytochrome P450 model. *J. Chem. Soc. Chem. Commun.* 1400–1401 (1982).
17. McIntosh, J. A. et al. Enantioselective intramolecular C–H amination catalyzed by engineered cytochrome P450 enzymes in vitro and in vivo. *Angew. Chem. Int. Ed.* **52**, 9309–9312 (2013).
18. Singh, R., Bordeaux, M. & Fasan, R. P450-catalyzed intramolecular sp^3 C–H amination with arylsulfonyl azide substrates. *ACS Catal.* **4**, 546–552 (2014).

19. Hyster, T. K., Farwell, C. C., Buller, A. R., McIntosh, J. A. & Arnold, F. H. Enzyme-controlled nitrogen-atom transfer enables regiodivergent C–H amination. *J. Am. Chem. Soc.* **136**, 15505–15508 (2014).
20. Singh, R., Kolev, J. N., Sutera, P. A. & Fasan, R. Enzymatic C(sp^3)–H amination: P450-catalyzed conversion of carbonazidates into oxazolidinones. *ACS Catal.* **5**, 1685–1691 (2015).
21. Steck, V., Kolev, J. N., Ren, X. K. & Fasan, R. Mechanism-guided design and discovery of efficient cytochrome P450-derived C–H amination biocatalysts. *J. Am. Chem. Soc.* **142**, 10343–10357 (2020).
22. Yang, Y., Cho, I., Qi, X. T., Liu, P. & Arnold, F. H. An enzymatic platform for the asymmetric amination of primary, secondary and tertiary C(sp^3)–H bonds. *Nat. Chem.* **11**, 987–993 (2019).
23. Prier, C. K., Zhang, R. J. K., Buller, A. R., Brinkmann-Chen, S. & Arnold, F. H. Enantioselective, intermolecular benzylic C–H amination catalysed by an engineered iron-haem enzyme. *Nat. Chem.* **9**, 629–634 (2017).
24. Athavale, S. V. et al. Biocatalytic, intermolecular C–H bond functionalization for the synthesis of enantioenriched amides. *Angew. Chem. Int. Ed.* **60**, 24864–24869 (2021).
25. Liu, Z. et al. An enzymatic platform for primary amination of 1-aryl-2-alkyl alkynes. *J. Am. Chem. Soc.* **144**, 80–85 (2022).
26. Dydio, P., Key, H. M., Hayashi, H., Clark, D. S. & Hartwig, J. F. Chemoselective, enzymatic C–H bond amination catalyzed by a cytochrome P450 containing an Ir(Me)-PIX cofactor. *J. Am. Chem. Soc.* **139**, 1750–1753 (2017).
27. Goldberg, N. W., Knight, A. M., Zhang, R. J. K. & Arnold, F. H. Nitrene transfer catalyzed by a non-heme iron enzyme and enhanced by non-native small-molecule ligands. *J. Am. Chem. Soc.* **141**, 19585–19588 (2019).
28. Vila, M. A., Steck, V., Giordano, S. R., Carrera, I. & Fasan, R. C–H amination via nitrene transfer catalyzed by mononuclear non-heme iron-dependent enzymes. *ChemBioChem* **21**, 1981–1987 (2020).
29. van Vliet, K. M. & de Bruin, B. Dioxazolones: stable substrates for the catalytic transfer of acyl nitrenes. *ACS Catal.* **10**, 4751–4769 (2020).
30. Biegasiewicz, K. F. et al. Photoexcitation of flavoenzymes enables a stereoselective radical cyclization. *Science* **364**, 1166–1169 (2019).
31. Black, M. J. et al. Asymmetric redox-neutral radical cyclization catalysed by flavin-dependent 'ene'-reductases. *Nat. Chem.* **12**, 71–75 (2020).
32. Zhou, Q., Chin, M., Fu, Y., Liu, P. & Yang, Y. Stereodivergent atom-transfer radical cyclization by engineered cytochromes P450. *Science* **374**, 1612–1616 (2021).
33. Rumo, C. et al. An artificial metalloenzyme based on a copper heteroscorpionate enables sp^3 C–H functionalization via intramolecular carbene insertion. *J. Am. Chem. Soc.* **144**, 11676–11684 (2022).
34. Kweon, J. & Chang, S. Highly robust iron catalyst system for intramolecular C(sp^3)–H amidation leading to γ-lactams. *Angew. Chem. Int. Ed.* **60**, 2909–2914 (2021).
35. Bordeaux, M., Tyagi, V. & Fasan, R. Highly diastereoselective and enantioselective olefin cyclopropanation using engineered myoglobin-based catalysts. *Angew. Chem. Int. Ed.* **54**, 1744–1748 (2015).
36. Bordeaux, M., Singh, R. & Fasan, R. Intramolecular C(sp^3)–H amination of arylsulfonyl azides with engineered and artificial myoglobin-based catalysts. *Bioorg. Med. Chem.* **22**, 5697–5704 (2014).
37. Pineda-Knauseder, A. J., Vargas, D. A. & Fasan, R. Organic solvent stability and long-term storage of myoglobin-based carbene transfer biocatalysts. *Biotechnol. Appl. Biochem.* **67**, 516–526 (2020).
38. Deng, T. et al. Rh_2(II)-catalyzed intermolecular *N*-aryl aziridination of olefins using nonactivated N atom precursors. *J. Am. Chem. Soc.* **143**, 19149–19159 (2021).
39. Sangster, J. J., Marshall, J. R., Turner, N. J. & Mangas-Sanchez, J. New trends and future opportunities in the enzymatic formation of C–C, C–N, and C–O bonds. *ChemBioChem* **23**, e202100464 (2022).
40. Mai, B. K., Neris, N. M., Yang, Y. & Liu, P. C–N bond forming radical rebound is the enantioselectivity-determining step in P411-catalyzed enantioselective C(sp^3)–H amination: a combined computational and experimental investigation. *J. Am. Chem. Soc.* **144**, 11215–11225 (2022).
41. Lang, K., Hu, Y., Lee, W.-C. L. & Zhang, X. P. Combined radical and ionic approach for the enantioselective synthesis of β-functionalized amines from alcohols. *Nat. Synth.* **1**, 548–557 (2022).
42. Tinoco, A. et al. Origin of high stereocontrol in olefin cyclopropanation catalyzed by an engineered carbene transferase. *ACS Catal.* **9**, 1514–1524 (2019).
43. Crombie, L., Haigh, D., Jones, R. C. F. & Matzin, A. R. Synthesis of the alkaloid homaline in (±) and natural (*S*,*S*)-(−) forms, using amination and transamidative ring expansion in liquid-ammonia. *J. Chem. Soc. Perkin Trans. 1* 2047–2054 (1993).
44. Chincholkar, P. M., Kale, A. S., Gumaste, V. K. & Deshmukh, A. R. A. S. An efficient formal synthesis of (*S*)-dapoxetine from enantiopure 3-hydroxy azetidin-2-one. *Tetrahedron* **65**, 2605–2609 (2009).
45. Wang, J. P., Gao, H., Yang, L. J. & Gao, Y. Q. Role of engineered iron-haem enzyme in reactivity and stereoselectivity of intermolecular benzylic C–H bond amination. *ACS Catal.* **10**, 5318–5327 (2020).
46. Kalita, S., Shaik, S. & Dubey, K. D. MD simulations and QM/MM calculations reveal the key mechanistic elements which are responsible for the efficient C–H amination reaction performed by a bioengineered P450 enzyme. *Chem. Sci.* **12**, 14507–14518 (2021).
47. Bajaj, P., Sreenilayam, G., Tyagi, V. & Fasan, R. Gram-scale synthesis of chiral cyclopropane-containing drugs and drug precursors with engineered myoglobin catalysts featuring complementary stereoselectivity. *Angew. Chem. Int. Ed.* **55**, 16110–16114 (2016).
48. Ren, X. K., Chandgude, A. L. & Fasan, R. Highly stereoselective synthesis of fused cyclopropane-γ-lactams via biocatalytic iron-catalyzed intramolecular cyclopropanation. *ACS Catal.* **10**, 2308–2313 (2020).
49. Chandgude, A. L., Ren, X. & Fasan, R. Stereodivergent intramolecular cyclopropanation enabled by engineered carbene transferases. *J. Am. Chem. Soc.* **141**, 9145–9150 (2019).

Acknowledgements

This work was supported by the US National Institute of Health (grant no. GM098628, to R.F.) and Cancer Prevention and Research Institute of Texas (CPRIT, RR230018 to R.F.). R.F. acknowledges endowed professorship support from the Robert A. Welch Foundation. D.A.V. acknowledges support from the National Science Foundation Graduate Fellowship Program. K.N.H. acknowledges support from the US National Science Foundation (grant no. CHE-1764328), and the Natural Science Foundation of China (grant no. 22103060) provided the computational resources used in the QM analyses. We are grateful to W. Brennessel (University of Rochester) for assistance with the crystallographic analyses. MS and X-ray instrumentation at the University of Rochester are supported by US National Science Foundation (grant nos. CHE-0946653 and CHE-1725028) and the US National Institute of Health (grant no. S10OD030302).

Author contributions

D.A.V., S.R. and R.F. conceived the project and designed the experiments. S.R. and D.A.V. performed the experiments with guidance from R.F. K.N.H. mentored P.M., A.S. and L.Z. in the molecular dynamics and quantum mechanics calculations and contributed to the writing of the mechanistic parts of the paper. D.A.V., S.R., A.S.and R.F wrote the paper. All authors discussed the results and contributed to the final paper.

Competing interests

The authors have no competing interests.

Additional information

Supplementary information The online version contains supplementary material available at https://doi.org/10.1038/s41929-023-01068-2.

Correspondence and requests for materials should be addressed to K. N. Houk or Rudi Fasan.

Peer review information *Nature Catalysis* thanks Sabine Flitsch and the other, anonymous, reviewer(s) for their contribution to the peer review of this work.

nature research

Corresponding author(s): Rudi Fasan

Last updated by author(s): Dec 27, 2022

Reporting Summary

Nature Research wishes to improve the reproducibility of the work that we publish. This form provides structure for consistency and transparency in reporting. For further information on Nature Research policies, see our Editorial Policies and the Editorial Policy Checklist.

Statistics

For all statistical analyses, confirm that the following items are present in the figure legend, table legend, main text, or Methods section.

n/a	Confirmed
☐	☒ The exact sample size (*n*) for each experimental group/condition, given as a discrete number and unit of measurement
☐	☒ A statement on whether measurements were taken from distinct samples or whether the same sample was measured repeatedly
☒	☐ The statistical test(s) used AND whether they are one- or two-sided *Only common tests should be described solely by name; describe more complex techniques in the Methods section.*
☒	☐ A description of all covariates tested
☒	☐ A description of any assumptions or corrections, such as tests of normality and adjustment for multiple comparisons
☒	☐ A full description of the statistical parameters including central tendency (e.g. means) or other basic estimates (e.g. regression coefficient) AND variation (e.g. standard deviation) or associated estimates of uncertainty (e.g. confidence intervals)
☒	☐ For null hypothesis testing, the test statistic (e.g. *F*, *t*, *r*) with confidence intervals, effect sizes, degrees of freedom and *P* value noted *Give P values as exact values whenever suitable.*
☒	☐ For Bayesian analysis, information on the choice of priors and Markov chain Monte Carlo settings
☒	☐ For hierarchical and complex designs, identification of the appropriate level for tests and full reporting of outcomes
☒	☐ Estimates of effect sizes (e.g. Cohen's *d*, Pearson's *r*), indicating how they were calculated

Our web collection on statistics for biologists contains articles on many of the points above.

Software and code

Policy information about availability of computer code

Data collection	• NMR data were acquired on a Bruker DPX-500 (500 MHz) and Bruker DPX-400 (400 MHz) spectrometers running Topspin X version 1.3.10 • GC-MS data were acquired using GCsolution version 2.50 SU3 (Shimadzu) • GC-FID data were acquired using GCsolution version 231.00 (Shimadzu) • UV-VIS absorption data were acquired using UVProbe version 2.10 (Shimadzu) • Molecular Dynamics simulations were performed using the GPU code (pmemd) of the AMBER 18 package. All Density Functional Theory (DFT) calculations were carried out using Gaussian16, Revision C.01 software. • Density Functional Theory (DFT) calculations were carried out using Gaussian16. • Detailed information regarding all data collection is provided in the Supporting Information.
Data analysis	• NMR spectra were analyzed using MNova version 14.2.1-27684 • GC-MS data were analyzed using GCsolution version 2.50 SU3 • GC-FID data were analyzed using GCsolution version 231.00 (Shimadzu) • UV-VIS absorption data were acquired using UVProbe version 2.10 (Shimadzu) • Molecular Dynamics trajectories were analyzed using the set of programs and scripts included in the AmberTools module from Amber18 package. • Detailed information regarding all data collection is provided in the Supporting Information.

For manuscripts utilizing custom algorithms or software that are central to the research but not yet described in published literature, software must be made available to editors and reviewers. We strongly encourage code deposition in a community repository (e.g. GitHub). See the Nature Research guidelines for submitting code & software for further information.

Data

Policy information about availability of data

All manuscripts must include a data availability statement. This statement should provide the following information, where applicable:

- Accession codes, unique identifiers, or web links for publicly available datasets
- A list of figures that have associated raw data
- A description of any restrictions on data availability

Data relating to the materials and methods, experimental procedures, mechanistic studies and computational calculations, gas chromatography and NMR spectra are available in the Supporting Information. All small molecules crystal structures have been deposited in the Cambridge Crystallographic Data Centre (CCDC) as described in the main text. All data necessary to support the paper's conclusions based on the computational modeling is available in the main text and the Supporting Information. Geometries of all DFT optimized structures are reported in the Supporting Information.

Field-specific reporting

Please select the one below that is the best fit for your research. If you are not sure, read the appropriate sections before making your selection.

☒ Life sciences ☐ Behavioural & social sciences ☐ Ecological, evolutionary & environmental sciences

For a reference copy of the document with all sections, see nature.com/documents/nr-reporting-summary-flat.pdf

Life sciences study design

All studies must disclose on these points even when the disclosure is negative.

Sample size	Enzymatic reactions were repeated at least in duplicate from independent experiments with different batches of enzyme. Assay yields were typically within 10% deviation among each run, and enantioselectivity was almost identical in duplicate runs (within 1% error bar). No statistical method was performed to predetermine sample size. All presented data are representative results for at least two experiments that were performed independently on different days.
Data exclusions	No data collected in this data were excluded.
Replication	All samples were measured as technical replicates (n ≥ 2) and are representative results for at least two experiments that were performed independently on different days and that successfully replicated the presented results.
Randomization	Randomization was not applicable to this study. All reagents and catalysts were selected and the reaction conditions were carefully designed.
Blinding	Blinding was not applicable to this study. All experimental data were acquired using automated equipment and analyzed using computational software, eliminating human error.

Reporting for specific materials, systems and methods

We require information from authors about some types of materials, experimental systems and methods used in many studies. Here, indicate whether each material, system or method listed is relevant to your study. If you are not sure if a list item applies to your research, read the appropriate section before selecting a response.

Materials & experimental systems

n/a	Involved in the study
☒	☐ Antibodies
☒	☐ Eukaryotic cell lines
☒	☐ Palaeontology and archaeology
☒	☐ Animals and other organisms
☒	☐ Human research participants
☒	☐ Clinical data
☒	☐ Dual use research of concern

Methods

n/a	Involved in the study
☒	☐ ChIP-seq
☒	☐ Flow cytometry
☒	☐ MRI-based neuroimaging